Atmos. Chem. Phys., 25, 17747–17759, 2025
https://doi.org/10.5194/acp-25-17747-2025

Atmospheric Chemistry and Physics Open Access EGU

Measurement report: High contribution of N_2O_5 uptake to particulate nitrate formation in NO_2-limited urban areas

Ziyi Lin[1,2,3], Chuanyou Ying[4], Lingling Xu[1,2], Xiaoting Ji[1,2,3], Keran Zhang[1,2], Feng Zhang[2], Gaojie Chen[1,2,3], Lingjun Li[1,2,3], Chen Yang[1,2,3], Yuping Chen[1,2,3], Ziying Chen[1,2,3], and Jinsheng Chen[1,2]

[1]State Key Laboratory of Advanced Environmental Technology, Institute of Urban Environment, Chinese Academy of Sciences, Xiamen 361021, China
[2]Fujian Key Laboratory of Atmospheric Ozone Pollution Prevention, Institute of Urban Environment, Chinese Academy of Sciences, Xiamen 361021, China
[3]University of Chinese Academy of Sciences, Beijing 100049, China
[4]Fuzhou Research Academy of Environmental Sciences, Fuzhou 350013, China

Correspondence: Lingling Xu (linglingxu@iue.ac.cn) and Jinsheng Chen (jschen@iue.ac.cn)

Received: 30 July 2025 – Discussion started: 16 September 2025
Revised: 8 November 2025 – Accepted: 13 November 2025 – Published: 5 December 2025

Abstract. Particulate nitrate (pNO_3^-) is a major component of fine particles in Chinese urban areas. However, the relative contributions of pNO_3^- formation pathways in urban areas remain poorly quantified, particularly under the NO_2-limited regime that governs its formation (as defined by the NO_2/O_3 ratio), which hinders effective particulate pollution control. In this study, comprehensive winter field observations were conducted in urban Xiamen, Southeast China. We observed significantly elevated nighttime pNO_3^- levels concurrent with increased N_2O_5 concentrations. Quantification using an observation-constrained model revealed that N_2O_5 uptake contributed 51.2 % to total pNO_3^- formation, which was comparable to that of the $OH + NO_2$ reaction. The N_2O_5 uptake was found to be mainly driven by nocturnal NO_3 oxidation capacity (modulated by NO_2 and O_3 levels) rather than by heterogeneous reaction conditions. Sensitivity simulations further demonstrated that pNO_3^- formation rate was more sensitive to NO_x variations than to VOCs variations. Implementing NO_x control measures at nighttime was shown to effectively reduce pNO_3^- by abating N_2O_5 uptake while simultaneously preventing daytime O_3 increase. Our findings enhance the understanding of pNO_3^- formation in NO_2-limited urban areas and provide valuable insights for developing joint $PM_{2.5}$ and O_3 mitigation strategies.

1 Introduction

Fine particulate matter ($PM_{2.5}$) contributes to various atmospheric environmental issues, including visibility deterioration, radiative forcing change, and adverse impacts on human health (Seinfeld, 1989; Lelieveld et al., 2015). Among its chemical components, particulate nitrate (pNO_3^-) has attracted increasing attention due to its rising mass fraction in $PM_{2.5}$ and its nonlinear responses to emission mitigation strategies (Xie et al., 2022; Zhai et al., 2021; Li et al., 2021; Zhang et al., 2021; Zhou et al., 2022; Zong et al., 2022; Wang et al., 2020). The primary formation pathways of pNO_3^- include gas-phase oxidation through the reaction of hydroxyl radicals (OH) and nitrogen dioxides (NO_2) (R1 and R2), and heterogeneous uptake of dinitrogen pentoxide (N_2O_5) which is produced via NO_2 oxidation by nitrate radicals (NO_3) (R3–R5) (Brown and Stutz, 2012). It is well recognized that the $OH + NO_2$ reaction dominates in daytime, while N_2O_5 uptake dominates in nighttime. During nocturnal pNO_3^- formation, particulate chlorides can induce N_2O_5 heterogeneous uptake to produce $ClNO_2$, thereby competing with pNO_3^- formation.

$$OH(g) + NO_2(g) + M \rightarrow HNO_3(g) + M \quad \text{(R1)}$$

$$HNO_3(g) + NH_3(g) \rightleftharpoons NH_4NO_3(p) \quad \text{(R2)}$$

$$NO_2(g) + O_3(g) \rightarrow NO_3(g) \quad \text{(R3)}$$

$$NO_2(g) + NO_3(g) \rightleftharpoons N_2O_5(g) \quad \text{(R4)}$$

$$N_2O_5(g) + H_2O/Cl^-(p) \rightarrow (2-\varphi)NO_3^-(p) + \varphi ClNO_2(g) \quad \text{(R5)}$$

Many studies have focused on quantifying the potential formation pathways of pNO_3^- in urban areas of China. In major urban agglomerations such as the Beijing-Tianjin-Hebei (BTH) region (Chen et al., 2020; Ma et al., 2023; Zhao et al., 2023), Yangtze River Delta (YRD) (Sun et al., 2022; Zhai et al., 2023; Zhang et al., 2023b), and Pearl River Delta (PRD) (Yang et al., 2022; Niu et al., 2022; Cheng et al., 2024), pNO_3^- formation was typically dominated by the gas-phase oxidation of $OH + NO_2$. In contrast, under special conditions such as the COVID-19 pandemic and $PM_{2.5}$ pollution events (Yan et al., 2023; Zhai et al., 2023), N_2O_5 uptake became the main pathway. Previous research has demonstrated that the formation rate of pNO_3^- via N_2O_5 uptake is closely related to its precursor NO_2 and O_3, and the N_2O_5 formation can be classified into NO_2-limited and O_3-limited regimes based on the NO_2/O_3 ratio (Ma et al., 2023). The winter NO_2/O_3 ratios in the BTH, YRD, and PRD regions were generally above 1, placing N_2O_5 formation in the O_3-limited or transition regime (Ma et al., 2023; Wen et al., 2018; Li et al., 2021; Zhang et al., 2023b). However, the N_2O_5 uptake served as the dominant pathway for pNO_3^- formation, typically under NO_2-limited conditions (e.g., reduced emissions during the pandemic) or under large aerosol surface areas (e.g., severe particulate pollution episodes). Collectively, these findings indicate that spatial variations in NO_2 and O_3 levels are likely a key driver of regional differences in the dominant formation pathways of pNO_3^-. The formation of pNO_3^- primarily depends on precursors OH, NO_2, and O_3, with OH and O_3 concentrations being influenced by VOCs and NO_x emissions. Thus, the different formation pathways of pNO_3^- result in complex responses to NO_x/VOCs emissions. The response of pNO_3^- formation via $OH + NO_2$ to precursors variation is relatively well-understood, as most Chinese urban areas are located in VOC-limited regimes for O_3 (Wang et al., 2023a, 2022c; Zhang et al., 2023a; Mao et al., 2022), and ammonia-rich regimes for pNO_3^- (Xing et al., 2018; Sun et al., 2022; Fu et al., 2024; Liu et al., 2019). Under these conditions, VOCs reduction suppresses pNO_3^- formation by decreasing OH concentrations, whereas NO_x reduction enhances pNO_3^- formation by weakening the NO_x titration effect. Given the regional variations in the NO_2/O_3 ratio across urban areas of China (Ma et al., 2023), the response of pNO_3^- formation via N_2O_5 uptake to precursor changes (VOCs, O_3) likely exhibits spatial heterogeneity. A recent study has revealed that under O_3-limited conditions for N_2O_5 formation (Zhang et al., 2023b), reducing NO_x emissions had negligible effects, while reducing VOCs decreased the consumption of NO_3 by VOCs, thereby enhancing pNO_3^- formation from N_2O_5 uptake. However, the response of pNO_3^- formation to precursors under NO_2-limited conditions remains unclear. Aside from precursor availability, N_2O_5 uptake is also greatly influenced by heterogeneous reaction conditions like aerosol composition and aerosol surface area (Mcduffie et al., 2018b, a; Tham et al., 2018; Yu et al., 2020), which introduces additional uncertainty in determining the contribution of pNO_3^- formation pathways and the effectiveness of precursor control strategies.

The NO_2/O_3 ratios in southeastern China predominantly fell within the NO_2-limited regime for N_2O_5 formation (Ma et al., 2023). Xiamen, as one of the most developed cities in southeastern China, exhibits relatively better air quality with low levels of VOCs and NO_x compared to China's megacities (Table S1 in the Supplement). This pattern well represents the future urban atmospheric conditions following the implementation of air pollution control measures in China. From December 2022–February 2023, we conducted comprehensive multi-parameter observations in urban Xiamen, including N_2O_5 and related chemical constituents. An observation-constrained box model incorporating the heterogeneous reaction parameters was utilized to quantify the rates of different pNO_3^- formation pathways. An explainable machine learning (ML) method was applied to identify the driving factors for high pNO_3^- formation rate via N_2O_5 uptake. Additionally, multi-scenario simulations were performed to examine the joint responses of pNO_3^- and O_3 formation to various NO_x and VOCs emissions. These findings enhance our understanding of pNO_3^- formation pathways and their environmental implications in NO_2-limited regions, providing valuable insights for developing joint $PM_{2.5}$ and O_3 mitigation strategies.

2 Methods

2.1 Field observation

Field observations were conducted during the winter period from 1 December 2022–3 February 2023, at an urban site (marked by the red star in Fig. S1 in the Supplement) in Xiamen, which is located in the southeastern coastal region of China. Detailed site information has been described in our previous studies (Yang et al., 2023; Liu et al., 2022). Trace gases (including PAN, HCHO, HONO, VOCs, O_3, NO_x, CO, and SO_2), chemical components in $PM_{2.5}$ (including organic carbon and elemental carbon, SO_4^{2-}, NO_3^-, NH_4^+, Cl^-), $PM_{2.5}$ mass concentration, and meteorological parameters (including ambient temperature (T), relative humidity (RH), atmospheric pressure (P), wind speed (WS), wind direction (WD), and photolysis rates) were continuously measured during the campaign. Detailed information about measurement methods and instruments is summarized in Sect. S1 in the Supplement. In addition, boundary layer height (BLH)

data were obtained from the ERA5 dataset (Hersbach et al., 2020).

A chemical ionization time-of-flight mass spectrometer equipped with an iodide source (iodide-TOF-CIMS, Aerodyne Research Inc., USA) was deployed to measure N_2O_5 and $ClNO_2$. A nearly 2 m long perfluoroalkoxy (PFA) tube with a 1/4-inch inner diameter was used for sampling. The total sampling flow rate was set as 10 standard liters per minute (SLPM), of which only 2SLPM was diverted to the CIMS. A nitrogen (N_2) flow (99.999 %, 2.7 SLPM), carrying methyl iodide (CH_3I) vapor released from a heated permeation tube, passed through a soft X-ray source (Tofwerk AG, P-type) to generate reagent ions I^-. The I^- was combined with the target gas in an ion molecule reaction (IMR) chamber and then detected by the ToF-CIMS. Ambient N_2O_5 and $ClNO_2$ were detected as the $I(N_2O_5)^-$ and $I(ClNO_2)^-$ clusters at 235 and 208 m/z. The detailed calibration procedures of N_2O_5 and $ClNO_2$ are described in Sect. S2, following established methods (Wang et al., 2022b, a; Thaler et al., 2011). Briefly, N_2O_5 was generated from the reaction between O_3 and excessive NO_2, while $ClNO_2$ was synthesized via the reaction of Cl_2 (6 ppm in N_2) with a moist mixture of $NaNO_2$ and NaCl. The calibration curves for N_2O_5 and $ClNO_2$ at different RH are shown in Fig. S2, with mean sensitivities of 0.110 ± 0.063 and 0.055 ± 0.018 ncps ppb^{-1}, respectively. The instrument background was determined by introducing dry N_2 into the inlet for 20 min. Based on three times the standard deviation (3σ) of the background signal, the typical 1 min detection limits for N_2O_5 and $ClNO_2$ were estimated to be 0.61 and 1.3 ppt, respectively.

2.2 Determination of pNO_3^- formation rate

The iterative box model developed by Wagner et al. with a simplified mechanism was employed to obtain key parameters of the N_2O_5 uptake process (Wagner et al., 2013), including the loss rate of N_2O_5 (kN_2O_5) and the production yield of $ClNO_2$ ($\varphi ClNO_2$, see in Sect. S3). To validate the iterative box model results, these parameters were calculated concurrently based on the classical steady-state approximation method (Sect. S4) (Brown et al., 2003; Chen et al., 2022). The derived parameters of N_2O_5 uptake were adopted for subsequent multiphase box model.

A Framework for 0-D Atmospheric Modeling (F0AM), incorporating the Master Chemical Mechanism (MCM v3.3.1) and heterogeneous mechanisms (Table S2), was employed to simulate nitrate formation rates for each day during the study period (Wolfe et al., 2016; Atkinson and Arey, 2003; Jenkin et al., 2015). The heterogeneous parameters derived from the iterative box model were implemented in F0AM. In addition, hourly interval data of trace gases, photochemically active species, meteorological variables, and reanalysis data were also applied to constrain the multiphase chemical box model. Detailed model configurations are provided in Sect. S5. As shown in Fig. S3, the model performed well in simulating the trends of N_2O_5 and $ClNO_2$ with R^2 of 0.88 and 0.49, respectively. However, a systematic underestimation existed in the simulated N_2O_5 and $ClNO_2$ concentrations, which likely resulted from the model configuration including overestimated physical removal rates, elevated concentration of intermediate VOC species, or uncertainties in transport processes. Consequently, the simulated pNO_3^- formation from N_2O_5 uptake in this study could be regarded as a lower limit. The simulated OH concentrations agreed well with parameterized method suggested by Ehhalt and Rohrer (Fig. S4, $R^2 = 0.86$) (Ehhalt and Rohrer, 2000). Based on model simulation and precursor observations, we quantified pNO_3^- formation rates through both $OH + NO_2$ and N_2O_5 uptake pathways by model integral.

2.3 Identification of influencing factors for pNO_3^- formation via N_2O_5 uptake

Extreme gradient boosting (XGBoost), a machine learning technique, has been widely applied in atmospheric chemistry research (Gui et al., 2020; Wang et al., 2023b; Requia et al., 2020). Here, we built a XGBoost model to reproduce the pNO_3^- formation rate via N_2O_5 uptake with selected variables. The model was built using the "xgboost" library (https://github.com/dmlc/xgboost/tree/master, last access: 8 November 2025) in a python environment. Explanatory variables included meteorological parameters (BLH, T, and RH), nocturnal atmospheric oxidation capacity $P(NO_3)$ calculated by $k_{NO_2+O_3}[NO_2][O_3]$, TVOCs, the logarithm of the ratio of NO_2 to O_3 ($\log([NO_2]/[O_3])$, NO, and heterogeneous uptake parameters ($\varphi ClNO_2$ and kN_2O_5). Only nighttime (18:00–06:00 LT the next day) data were considered to identify key drivers of pNO_3^- formation via N_2O_5 uptake. The hyperparameters of the XGBoost model were tuned by grid searching method and the established model was evaluated using R^2, Mean Absolute Error (MAE) and Root Mean Square Error (RMSE). By incorporating SHAP interpretation, the XGBoost-SHAP method could quantify factor contributions through SHAP values, where absolute SHAP values denote the relative importance. Detailed description and setup of the XGBoost-SHAP method can be found in Sect. S6 and our previous study (Lin et al., 2024).

2.4 Emission scenario modelling

Using the aforementioned multiphase chemical box model, we investigated changes in formation rates of pNO_3^- (PNO_3^-) and O_3 (PO_3) under different VOCs and NO_x emission scenarios. The base model simulation was performed using mean diurnal values from the winter 2022 observations. A series of emission scenarios were tested by scaling normalized VOCs and NO_x concentrations from 0–2 times baseline levels to examine their impacts on PNO_3^- and PO_3. Prior to each scenario simulation, 3d spin-up was set to stabilize intermediate species concentrations. Isopleth diagrams of sim-

ulated PNO_3^- and PO_3 were obtained from the base scenario and 120 emission change scenarios. In addition, response strength (RS) was calculated using Eq. (2) as an indicator of emission sensitivity.

$$PO_3 = k_1[HO_2][NO] + \sum k_{2i}[RO_2][NO] \quad (1)$$

where, k_i is the corresponding chemical reaction rate constants.

$$RS = \frac{X_i - X_{base}}{V_i - V_{base}} \quad (2)$$

where, X_i and X_{base} are the mean formation rates of dependent variables e.g. PNO_3^-, PO_3 in scenario i and base simulations, respectively. V_i and V_{base} are the emission rates for the scenario i and base simulations, respectively. Notably, the emission rates ranged from 0–2 times baseline levels, with the base simulation emission rate normalized to 1.

3 Results and discussion

3.1 Overview of observations

The mean diurnal patterns of pNO_3^-, gaseous pollutants and relevant meteorological parameters are shown in Fig. 1. During the entire observation period, mean concentrations of NO_2, O_3, total VOCs, and $PM_{2.5}$ were 10.9 ppb, 27.3 ppb, 18.2 ppb, and 14.3 $\mu g\,m^{-3}$, respectively, lower than those observed in most of China's key cities (refer to Table S1). Despite the low NO_x levels, pNO_3^- contributed 29.5 % to $PM_{2.5}$ mass concentration, which was higher than proportions reported in Beijing urban area (24.7 %) (Ma et al., 2023), Guangdong (24.0 %) (Yun et al., 2018), and Nanjing (24 %–27 %) (Huang et al., 2020). This discrepancy suggests efficient conversion from NO_2 to pNO_3^- in the study area. In addition, the proportion of pNO_3^- increased with rising $PM_{2.5}$ concentration (Fig. S6), indicating its importance to particulate pollution. This is consistent with the phenomenon widespread in urban areas of China where pNO_3^- became dominant in inorganic aerosols despite NO_x reduction, underscoring the need for efficient pNO_3^- control strategies (Zhai et al., 2021; Zhao et al., 2020; Zhang et al., 2022).

The diurnal pattern of pNO_3^- exhibited a bimodal characteristic, with peaks occurring at 04:00 and 15:00 LT, respectively. The daytime peak (07:00–17:00 LT was accompanied by low concentrations of NO_x and high levels of O_3 and JNO_2, indicating that active photochemical conditions promoted daytime pNO_3^- formation. During the nighttime (18:00–06:00 LT the next day), pNO_3^- concentrations increased together with NO_2, N_2O_5 and $ClNO_2$ from 18:00 LT onward and remained elevated until early morning. This nighttime accumulation can be attributed to two factors. First, lower temperature, shallower boundary layer height, and reduced wind speed at night favored the accumulation of pNO_3^- and related nitrogen-containing species. Second, higher RH and $PM_{2.5}$ concentrations at night enhanced

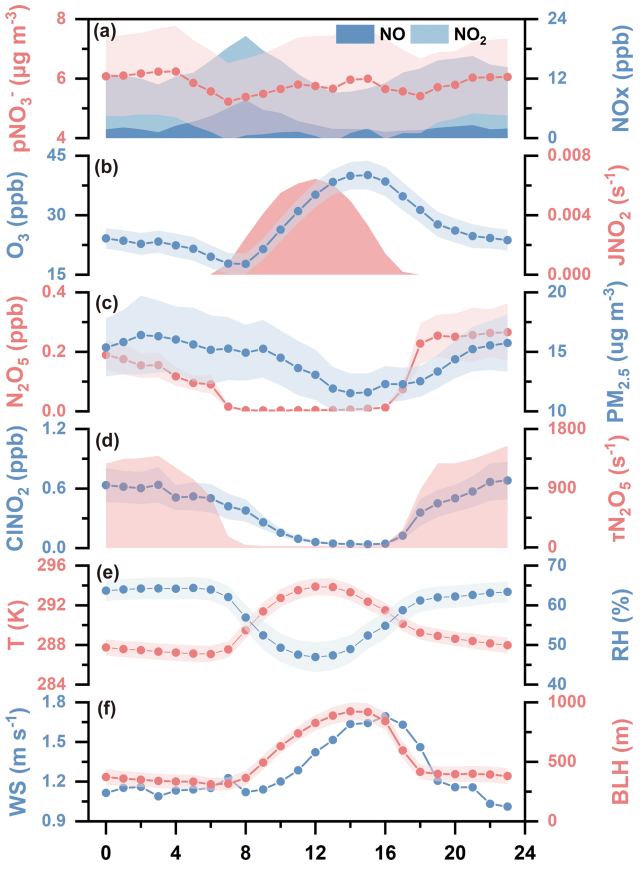

Figure 1. Diurnal variations of key parameters during the winter of 2022. The concentrations of pNO_3^-, NO_x, O_3, N_2O_5, $PM_{2.5}$ and $ClNO_2$. The levels of the photolysis frequencies of NO_2 (JNO_2), ambient temperature (T), relative humidity (RH), the lifetime of N_2O_5 (τN_2O_5), wind speed (WS) and the boundary layer height (BLH). Shaded areas of pNO_3^-, O_3, N_2O_5, $PM_{2.5}$, $ClNO_2$, T, RH and BLH represent 95 % confidence intervals.

aerosol water content and surface area, providing favorable conditions for heterogeneous hydrolysis of N_2O_5 to form pNO_3^-. The mean concentration of N_2O_5 was 0.19±0.26 ppb (peaking at 2.52 ppb), which is relatively higher than values reported for China's megacities (Chen et al., 2020; Wang et al., 2017; Tham et al., 2018; Wang et al., 2022a; Liu et al., 2025; Li et al., 2023). Moreover, the observed elevation in nighttime $ClNO_2$, primarily produce via the reaction of N_2O_5 with Cl-containing particles, strongly supports the presence of active heterogeneous processes of N_2O_5. Collectively, these findings imply a likely significant contribution of N_2O_5 uptake to pNO_3^- formation during the nighttime.

3.2 High contribution of N_2O_5 uptake to pNO_3^- formation in NO_2-limited conditions

In view of the observed importance of daytime and nighttime pNO_3^- formation, we further employed an observation-constrained model to quantify the potential formation path-

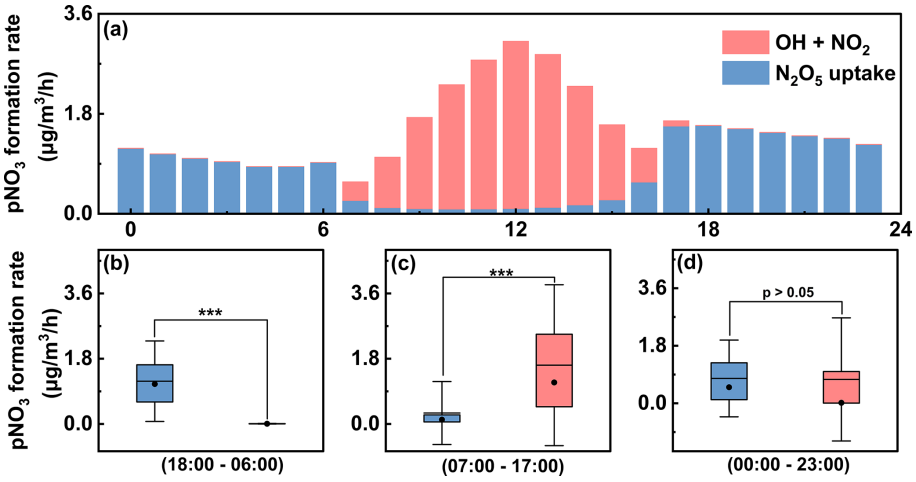

Figure 2. Simulated rates of key pNO_3^- formation pathways obtained from the chemical box model incorporating heterogeneous parameters. Diurnal formation rates of pNO_3^- via the OH+NO_2 and N_2O_5 uptake pathways **(a)** and comparison of the two pathways during the nighttime **(b)**, daytime **(c)**, and the whole day **(d)**. Note that the results in panel **(a)** represent the mean simulated formation rates over the entire observation period. The box shows the 25th–75th percentiles with whiskers representing the 5th–95th percentiles. The black line and dot inside the box represent the mean and median values, respectively. Statistical significance was determined using pair-sample *t*-tests with *** indicating $p < 0.001$.

ways, including the gas-phase reaction of OH+NO_2 and heterogeneous N_2O_5 uptake. This model incorporated heterogeneous chemical mechanisms, with key heterogeneous parameters (e.g. kN_2O_5 and $\varphi ClNO_2$) obtained through simulation (See Methods for details). As shown in Fig. S7, the simulated kN_2O_5 and $\varphi ClNO_2$ exhibited good agreement with the classical steady-state method ($R^2 = 0.76$ and 0.73, respectively), demonstrating the model's capability to characterize heterogeneous uptake processes and thereby effectively evaluate pNO_3^- formation processes.

As illustrated in Fig. 2a, the diurnal pattern of pNO_3^- formation rates exhibited a classical characteristic, with daytime dominated by gas-phase oxidation and nighttime dominated by N_2O_5 uptake. Specifically, the daytime OH + NO_2 reaction had a mean pNO_3^- formation rate of 1.62 $\mu g\,m^{-3}\,h^{-1}$, while the nighttime N_2O_5 uptake pathway showed a formation rate of 1.18 $\mu g\,m^{-3}\,h^{-1}$ (Fig. 2b and c). For the whole day, N_2O_5 uptake contributed an average of 51.2 % to pNO_3^- formation, which was comparable to the contribution of the OH + NO_2 pathway (Fig. 2d). To exclude year-specific effects, we further analyzed pNO_3^- formation during the winters from 2019–2023. The results revealed that the pNO_3^- formation rates via N_2O_5 uptake (0.75–1.40 $\mu g\,m^{-3}\,h^{-1}$) were comparable to those from the OH+NO_2 reaction (0.88–1.66 $\mu g\,m^{-3}\,h^{-1}$; Fig. 3a), with the N_2O_5 uptake pathway consistently accounting for approximately half of the total pNO_3^- formation in the study area (Fig. 3b). Such a high contribution of N_2O_5 uptake to pNO_3^- is generally uncommon in urban areas. A study in urban Beijing showed that during non-polluted periods, N_2O_5 uptake contributed only 18.9 % to nitrate formation rates (Ma et al., 2023). Similarly, the contributions of N_2O_5 uptake were 10 %–38 % and 4 % in urban areas of the YRD (Sun et al., 2022; Zhai et al., 2023; Zhang et al., 2023b) and PRD regions(Yang et al., 2022), respectively.

Previous studies have found that nocturnal pNO_3^- formation via N_2O_5 uptake strongly depends on the ratio of NO_2 to O_3 (Ma et al., 2023). This process is suppressed in the O_3-limited regime ($NO_2/O_3 > 2$) but enhanced in the NO_2-limited regime ($NO_2/O_3 \leq 1$). The COVID-19 lockdown period was a typical example of this ratio dependence(Yan et al., 2023). In regions like Beijing, substantial reductions in NO_x emissions caused a shift in nocturnal pNO_3^- formation from the O_3-limited to the NO_2-limited regime. This shift resulted in elevated nighttime O_3 levels and a weakened NO titration effect, collectively promoting N_2O_5 formation and subsequent pNO_3^- formation. The sensitivity of pNO_3^- formation via N_2O_5 uptake to NO_2 and O_3 during the campaign is presented in Fig. 3c and d. The observed mean values of NO_2/O_3 (0.40) and the probability distributions of NO_2/O_3 ratios both indicate that N_2O_5 uptake was in the NO_2-limited regime. Based on NO_2 and O_3 observational data during 2015–2021 from the China National Environmental Monitoring Centre(Ma et al., 2023), most key urban regions in China (e.g., the NCP, YRD, and Beijing) were found to lie in the O_3-limited or transition regimes ($1 < NO_2/O_3 \leq 2$), whereas nocturnal pNO_3^- formation in southeastern China was distinctly in NO_2-limited regime. These results confirm that the dominant pNO_3^- formation mechanisms in our study area significantly differs from those in most urban areas of China, which might be attributed to the dependence of N_2O_5 uptake on precursor NO_2 and O_3. In addition, the dominance of

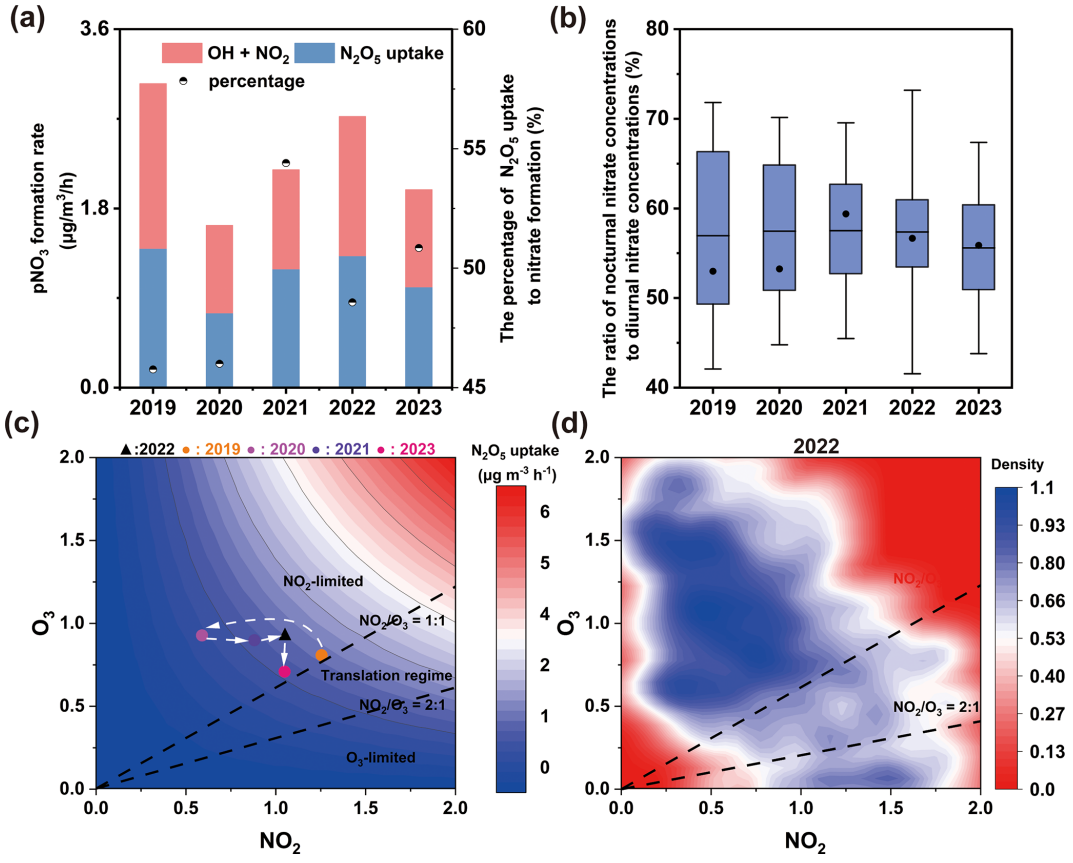

Figure 3. Inter-annual patterns of key pNO_3^- formation pathways in urban Xiamen. The average pNO_3^- formation rate from $OH + NO_2$ and N_2O_5 uptake **(a)**, and the average ratio of the sum of nocturnal pNO_3^- concentrations to the sum of all-day pNO_3^- concentration **(b)** in different winters from 2019–2023 based on the measured pNO_3^- in $PM_{2.5}$. The sensitivity of nocturnal pNO_3^- formation via N_2O_5 uptake to NO_2 and O_3 from 2019–2023 **(c)**. And probability distribution of observed NO_2/O_3 at nighttime in winter 2022 **(d)**. The observed periods of different winters from 2019–2023 are summarized in Table S3. In panel **(b)**, the black line and the solid circle in the boxplot represent the mean and median value, respectively. In panel **(c)**, the black triangle indicates the base case of winter 2022, solid circles in different colors represent the average NO_2 to O_3 ratios in different years, and the predicted average formation rate of N_2O_5 uptake as the normalized emissions (average concentrations of O_3 and NO_2) varied between 0–2.

N_2O_5 uptake in pNO_3^- formation also occurred during haze pollution periods (Zhai et al., 2023; Wang et al., 2017), where increased aerosol surface area under high particulate loadings created favorable conditions for N_2O_5 heterogeneous reactions. Therefore, to evaluate the role of precursors, we conducted a comprehensive analysis of the factors driving pNO_3^- formation via N_2O_5 uptake.

3.3 Driving factors of pNO_3^- formation via nocturnal N_2O_5 uptake

The N_2O_5 uptake rate is influenced by multiple factors including precursor levels, meteorological parameters, and heterogeneous reaction conditions (Ma et al., 2023; Chen et al., 2020, 2024). A machine learning method integrating these factors was employed to identify the key drivers of pNO_3^- formation via N_2O_5 uptake. The relative importance of each factor was evaluated by absolute SHAP values (Fig. 4a), and their impacts were elucidated by examining the relationships between individual factors and their corresponding SHAP values (Fig. 4b–e and S8). Results showed that the nocturnal NO_3 formation rate ($P(NO_3)$), an integrated indicator of nocturnal atmospheric oxidation capacity (Wang et al., 2021), was the most important factor. The steep slope of the positive correlation between $P(NO_3)$ and SHAP values indicated that $P(NO_3)$ strongly enhances pNO_3^- formation via N_2O_5 uptake. $P(NO_3)$ is primarily formed through the reaction between NO_2 and O_3 ($P(NO_3) = k_{NO_2+O_3}[NO_2][O_3]$), suggesting that NO_2 and O_3 mainly influenced pNO_3^- formation via N_2O_5 by modulating NO_3 radical formation. Notably, the factor $\log NO_2/O_3$ had relatively low importance, indicating concentrations of precursors were more important than NO_2/O_3 ratio in determining pNO_3^- formation via N_2O_5 uptake under extremely NO_2-limited condition (mean NO_2/O_3 was 0.40). Furthermore, as shown in

Fig. S8b, $\log NO_2/O_3$ and its SHAP value show a positive correlation when $\log NO_2/O_3$ is less than 0. This indicates that under NO_2-limited conditions ($\log NO_2/O_3 < 0$, i.e., $NO_2/O_3 < 1$), pNO_3^- formation via N_2O_5 uptake was driven by the elevated NO_2.

Compared with $P(NO_3)$, other factors exhibited weaker effects on pNO_3^- formation rate via N_2O_5 uptake. $\varphi ClNO_2$ emerged as the second most important factor and showed a negative correlation with SHAP values (Fig. 4c), illustrating that $ClNO_2$ formation inhibited pNO_3^- formation. This inhibitory effect could be attributed to high concentrations of Cl-containing particles ($0.94 \pm 1.11\,\mu g\,m^{-3}$) in the study area. Chloride-containing aerosols promote N_2O_5 uptake to produce more $ClNO_2$ (as evidenced by the positive correlation between $\varphi ClNO_2$ and chloride ions, Fig. S9), while simultaneously reducing pNO_3^- formation (R5). Additionally, the nighttime produced $ClNO_2$ can undergo photolysis in following day to release Cl radicals, which further promote O_3 formation. This indirect effect must be considered when formulating control measures for particulate matter pollution. Interestingly, as shown in Table S4 (Tham et al., 2016; Wang et al., 2018; Yun et al., 2018; Morgan et al., 2015), although the simulated kN_2O_5 ($7.64 \times 10^{-3} \pm 6.12 \times 10^{-3}\,s^{-1}$) was higher than values reported in Beijing ($8.1 \times 10^{-4} - 1.42 \times 10^{-3}\,s^{-1}$), Guangdong ($3.78 \times 10^{-3} - 9 \times 10^{-3}\,s^{-1}$), and UK ($9.3 \times 10^{-5} - 10^{-3}\,s^{-1}$), kN_2O_5 exerted only a weak positive effect on N_2O_5 uptake (Fig. 4d). The large difference existing in the importance of $P(NO_3)$ and kN_2O_5 indicated that the pNO_3^- formation rate via N_2O_5 uptake process was more limited by precursor levels rather than heterogeneous uptake conditions. Similar phenomenon was also found in winter in urban Beijing and Northern Utah mountain basins (Mcduffie et al., 2019; Chen et al., 2020). The total concentrations of the observed VOCs (TVOCs) showed a weak negative correlation with N_2O_5 uptake (Fig. 4e). Similar to existing research (Hu et al., 2023), specific VOC species, such as styrene, 2-butene, and isoprene, can readily consume NO_3 radicals (Fig. S10), thereby inhibiting N_2O_5 formation. However, the loss of N_2O_5 through the reaction between VOCs and NO_3 was relatively limited compared to its direct uptake, as determined by our calculations (Text S4), which supported the SHAP analysis.

Moreover, we found that the effects of $\varphi ClNO_2$, kN_2O_5, and TVOCs on pNO_3^- formation via N_2O_5 uptake were subject to $P(NO_3)$ levels (Fig. 5a–c). Specifically, the negative effect of $\varphi ClNO_2$ and the positive effect of kN_2O_5 on pNO_3^- formation via N_2O_5 uptake became statistically significant when $P(NO_3)$ exceeded approximately 1.0 and $0.5\,ppb\,h^{-1}$, respectively. The negative correlation slope of TVOCs versus pNO_3^- formation via N_2O_5 uptake intensified with increasing $P(NO_3)$ levels, indicating that the N_2O_5 removal effect was enhanced through VOC-induced NO_3 depletion. These findings highlight the critical role of precursor NO_2 and O_3 in nocturnal pNO_3^- formation, demonstrating that these precursors mainly affect this pathway by modulating NO_3 radical formation.

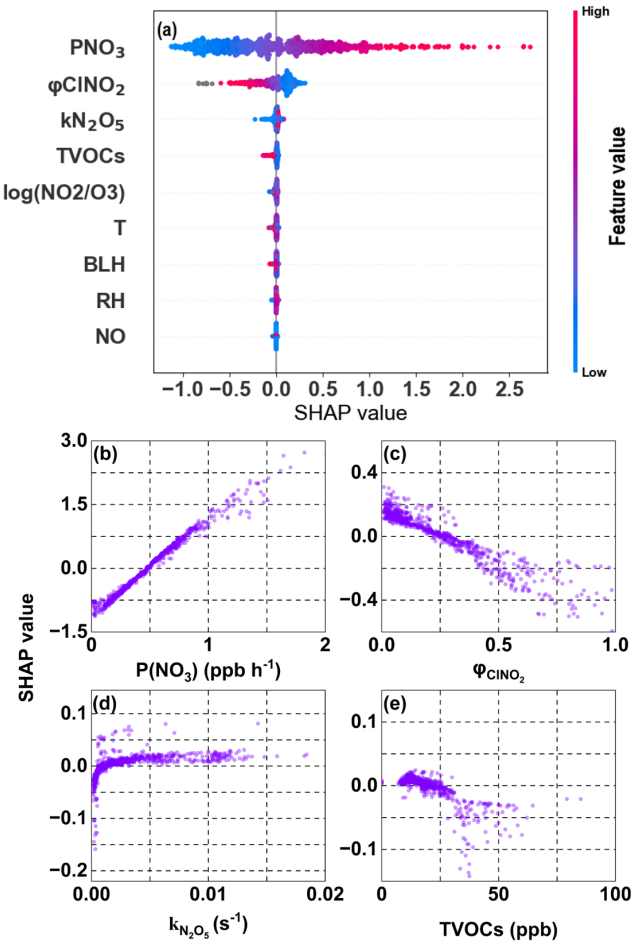

Figure 4. Feature importance **(a)** and the effects of key factors on pNO_3^- formation via N_2O_5 uptake **(b–e)** obtained by the XGBoost-SHAP method. The relationships between SHAP values and major features: $P(NO_3)$ **(b)**, $\varphi ClNO_2$**(c)**, kN_2O_5 **(d)**, and TVOCs **(e)**. Feature importance ranking **(a)** is determined by mean absolute SHAP values (descending order, top to bottom). Relationships between SHAP values and other factors are shown in Fig. S8.

3.4 Optimal mitigation strategies of pNO_3^- under NO_2-limited conditions

The above results revealed that pNO_3^- formation through both the daytime $OH + NO_2$ reaction and nocturnal heterogeneous N_2O_5 uptake was closely linked to VOCs–NO_x–O_3 chemistry (Yang et al., 2022). Using a multiphase box model, we systematically examined the responses of both pNO_3^- and O_3 to varying NO_x and VOC emission scenarios. Figure 6a shows pNO_3^- formation located in the transition regime of VOCs and NO_x. The formation rate of pNO_3^- (PNO_3^-) decreased with the reductions of VOCs and NO_x, and this trend became more pronounced under aggressive NO_x re-

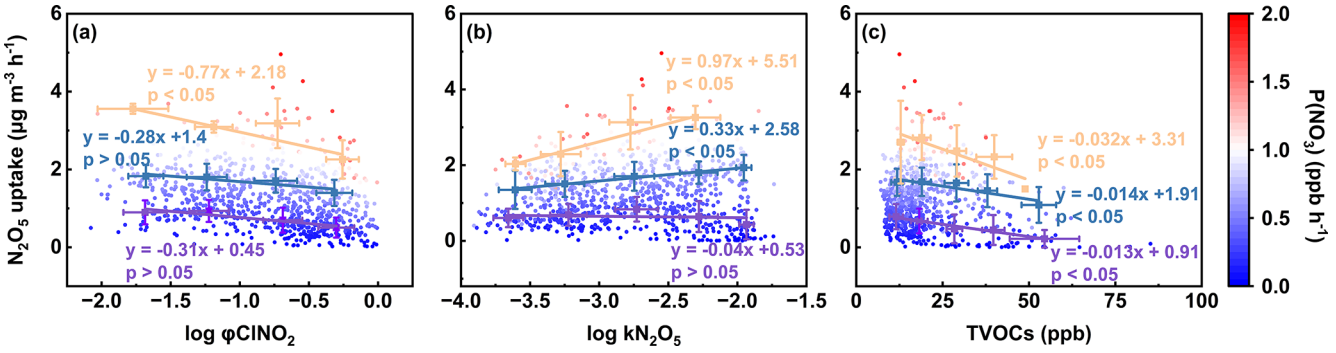

Figure 5. Relationships between pNO_3^- formation via N_2O_5 uptake and $\varphi ClNO_2$ **(a)**, kN_2O_5 **(b)**, and TVOCs **(c)** colored by $P(NO_3)$. Linear fit curves in purple, blue and orange represent the fitting results for $P(NO_3)$ in the ranges of 0–0.5, 0.5–1.0 and $> 1.0\,ppb\,h^{-1}$, respectively.

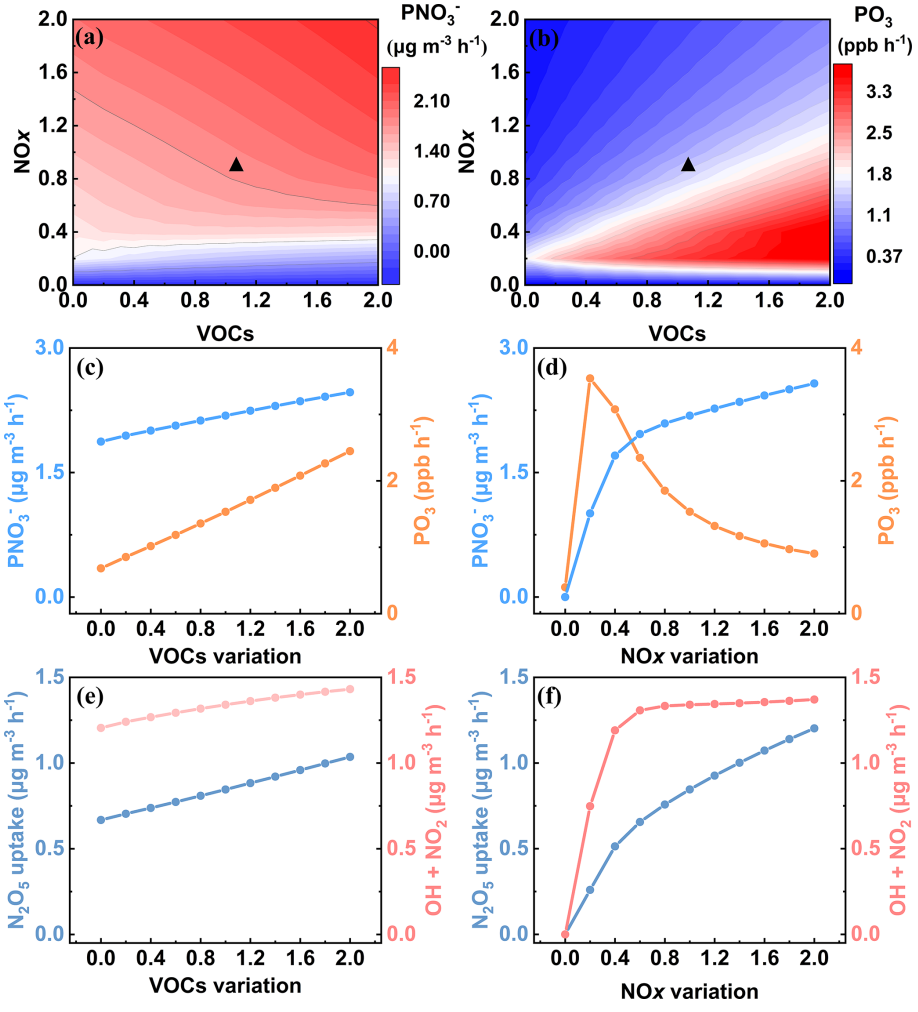

Figure 6. Results of multi-scenario simulations obtained from an observation-constrained box model. Isopleths of simulated PNO_3^- **(a)** and PO_3 **(b)** with normalized VOCs and NO_x. Simulated mean formation rates of pNO_3^- and O_3 **(c, d)**, as well as pNO_3^- formation rates via N_2O_5 uptake and $OH + NO_2$ **(e, f)** with normalized VOCs and NO_x. The PNO_3^- and PO_3 denote the formation rates of pNO_3^- and O_3, respectively. The simulated results are daily mean values, and the black triangle indicates the base case for winter 2022. In addition, the results in panel **(c–f)** were obtained by maintaining either NO_x or VOCs at the base emission rate while varying the other.

duction scenarios (Fig. 6c and d). Figure S11a and b reveal that the mean response strength (RS, as defined in Methods) of PNO_3^- to NO_x was 0.75, higher than that for VOCs (RS = 0.29), suggesting that NO_x reduction had a greater potential for pNO_3^- mitigation compared to VOCs control. However, NO_x and VOCs reductions exerted different impacts on O_3 formation rate (PO_3). In our study area, PO_3 located in the VOC-limited regime (Fig. 6b). We found that PO_3 declined with VOCs reduction but increased with NO_x reduction until NO_x dropped below 20 % of the base (Fig. 5c and d). Moreover, detailed results distinguishing daytime and nighttime major formation pathways of pNO_3^- are presented in Fig. 6e and f and Fig. S11c and d. For VOC reduction scenarios, both the $OH + NO_2$ reaction and N_2O_5 uptake pathways showed declining nitrate formation rates, with comparable RS of 0.11 and 0.18, respectively. This occurs because reduced VOCs concentrations decrease OH radical and O_3 concentrations, thereby suppressing pNO_3^- formation via both pathways. In contrast, NO_x reduction yielded more complex behavior. The $OH + NO_2$ reaction rates remained nearly constant until NO_x dropped to 60 % of the base. This stability arises because NO_x reduction diminishes the NO titration effect on O_3, thereby increasing OH radicals through O_3 photolysis. The competing effects of NO_x reduction and OH enhancement led to an initial plateau in the $OH + NO_2$ reaction rate before its eventual decline. Differently, the N_2O_5 uptake rate decreased consistently and significantly with NO_x abatement, exhibiting a high mean RS value of 0.61. This phenomenon was closely associated with the NO_2-limited regime of N_2O_5 uptake in the study area. As shown in Fig. S12, the variation trends of PNO_3^-, $P(O_3)$, $OH + NO_2$, and N_2O_5 uptake were consistent across all VOCs/NO_x combinations, indicating that the results robustly reflect the response mechanisms to precursor emission changes.

As mentioned above, while VOCs reduction proved effective in mitigating both pNO_3^- and O_3, its effectiveness in reducing pNO_3^- remained limited compared to NO_x reduction. However, the effectiveness of NO_x reduction exhibited significant regional and temporal variations. In China's megacities, including PRD, YRD, and BTH regions, pNO_3^- initially increased and then decreased in response to the reduction of NO_x emissions (Li et al., 2021; Zhang et al., 2023b; Yang et al., 2022). Under high-NO_x conditions, mild NO_x reduction would raise daytime OH and O_3 concentrations (Zhang et al., 2023b), rendering OH (rather than NO_x) the limiting factor for the $OH + NO_2$ reaction, which consequently enhanced daytime pNO_3^- formation. Additionally, as the season most susceptible to PM pollution, wintertime N_2O_5 formation in these regions was in an O_3-limited or transition regime (Ma et al., 2023), wherein the elevated daytime O_3 significantly enhanced NO_3 radical generation, thereby promoting nocturnal N_2O_5 uptake and subsequent pNO_3^- formation. Conversely, in NO_2-limited regions (e.g., southeastern China), NO_x reduction showed limited impact on daytime pNO_3^- formation via the $OH + NO_2$ pathway but effectively suppressed nighttime pNO_3^- formation via N_2O_5 uptake. This approach concurrently reduced $ClNO_2$ formation from N_2O_5 heterogeneous processes, consequently diminishing next-day Cl radical generation and its positive feedback on O_3 formation. Considering NO_x reduction during the daytime would cause O_3 formation and only a slight reduction in pNO_3^-, it is preferable to regulate NO_x at night (18:00–06:00 LT the next day). Our findings demonstrate that in regions with a NO_2-limited for pNO_3^- formation, targeted NO_x reduction can synergistically decrease both pNO_3^- and O_3 concentrations, highlighting the critical need to tailor mitigation strategies for different regions.

4 Conclusions and implications

Our observations revealed a bimodal diurnal pattern of pNO_3^- in winter in urban Xiamen. The co-occurrence of elevated nighttime pNO_3^- levels with increased N_2O_5 implied a significant contribution of N_2O_5 uptake to pNO_3^- formation. Quantitative model analysis showed that N_2O_5 uptake contributed 51.2 % of the total pNO_3^-, which was comparable to the $OH + NO_2$ reaction. This high contribution of N_2O_5 uptake to pNO_3^- is not commonly observed across Chinese cities. Comparative analysis among different cities suggests that this phenomenon is likely associated with NO_2-limited conditions for N_2O_5 uptake in our study area. Machine learning results further demonstrated that pNO_3^- formation via N_2O_5 uptake was driven by nocturnal atmospheric oxidation capacity (PNO_3) rather than heterogeneous uptake conditions. The underlying mechanism is that the weakened NO_x titration effects lead to nighttime O_3 accumulation, which promotes NO_3 radical generation and consequently enhances N_2O_5 and pNO_3^- formation. The joint response of pNO_3^- and O_3 to various NO_x and VOCs emission scenarios indicated that pNO_3^- was more sensitive to NO_x reduction than to VOCs reduction. However, mild NO_x reduction showed limited effectiveness in reducing daytime pNO_3^- while simultaneously increasing O_3 concentrations. Our findings suggest that NO_x reduction is more effective when implemented during nighttime, particularly in regions where N_2O_5 formation is NO_2-limited. This approach can effectively control pNO_3^- formation by suppressing nocturnal NO_3 radical generation and consequently inhibiting N_2O_5 uptake, while simultaneously alleviate O_3 pollution by reducing $ClNO_2$ formation. With continuous NO_x and VOCs emission reductions and renewable energy adoption in China, urban areas are transitioning from NO_x-saturated to NO_x-limited conditions, potentially increasing the importance of the N_2O_5 uptake pathway. In this context, comprehensive assessment of NO_x reduction impacts on urban pNO_3^- and O_3 pollution, along with the development of region-specific mitigation strategies, becomes critically important.

Code availability. Data analysis methods are available from the authors upon request.

Data availability. The dataset for this paper can be accessed at https://doi.org/10.6084/m9.figshare.29670629 (Lin et al., 2025).

Supplement. The supplement related to this article is available online at https://doi.org/10.5194/acp-25-17747-2025-supplement.

Author contributions. ZL contributed to the methodology, data curation, software, analysis and writing of the original draft. LX and JC contributed to the conceptualization, investigation, data curation, reviewing and editing the text, supervision, and funding acquisition. Ch. Y, XJ, KZ, FZ, GC, LL, CY, YC, and ZC provided useful advice and revised the manuscript.

Competing interests. The contact author has declared that none of the authors has any competing interests.

Disclaimer. Publisher's note: Copernicus Publications remains neutral with regard to jurisdictional claims made in the text, published maps, institutional affiliations, or any other geographical representation in this paper. While Copernicus Publications makes every effort to include appropriate place names, the final responsibility lies with the authors. Views expressed in the text are those of the authors and do not necessarily reflect the views of the publisher.

Acknowledgements. We acknowledge the data contributed by the field campaign team.

Financial support. This research has been supported by the National Natural Science Foundation of China (U22A20578), the guiding project of seizing the commanding heights of a "self-purifying city" (IUE-CERAE-202402), the National Key Research and Development Program (2022YFC3700304), the STS Plan Supporting Project of the Chinese Academy of Sciences in Fujian Province (2023T3013), and the Xiamen Atmospheric Environment Observation and Research Station of Fujian Province.

Review statement. This paper was edited by Eleanor Browne and reviewed by two anonymous referees.

References

Atkinson, R. and Arey, J.: Atmospheric degradation of volatile organic compounds, Chem. Rev., 103, 4605–4638, https://doi.org/10.1021/cr0206420, 2003.

Brown, S. S. and Stutz, J.: Nighttime radical observations and chemistry, Chem. Soc. Rev., 41, 6405–6447, https://doi.org/10.1039/c2cs35181a, 2012.

Brown, S. S., Stark, H., and Ravishankara, A. R.: Applicability of the steady state approximation to the interpretation of atmospheric observations of NO_3 and N_2O_5, J. Geophys. Res.-Atmos., 108, 4539, https://doi.org/10.1029/2003jd003407, 2003.

Chen, X., Wang, H., and Lu, K.: Interpretation of $NO_3-N_2O_5$ observation via steady state in high-aerosol air mass: the impact of equilibrium coefficient in ambient conditions, Atmos. Chem. Phys., 22, 3525–3533, https://doi.org/10.5194/acp-22-3525-2022, 2022.

Chen, X., Ma, W., Zheng, F. X., Wang, Z. C., Hua, C. J., Li, Y. R., Wu, J., Li, B. D., Jiang, J. K., Yan, C., Petäjä, T., Bianchi, F., Kerminen, V. M., Worsnop, D. R., Liu, Y. C., Xia, M., and Kulmala, M.: Identifying Driving Factors of Atmospheric N_2O_5 with Machine Learning, Environ. Sci. Technol., https://doi.org/10.1021/acs.est.4c00651, 2024.

Chen, X. R., Wang, H. C., Lu, K. D., Li, C. M., Zhai, T. Y., Tan, Z. F., Ma, X. F., Yang, X. P., Liu, Y. H., Chen, S. Y., Dong, H. B., Li, X., Wu, Z. J., Hu, M., Zeng, L. M., and Zhang, Y. H.: Field Determination of Nitrate Formation Pathway in Winter Beijing, Environ. Sci. Technol., 54, 9243–9253, https://doi.org/10.1021/acs.est.0c00972, 2020.

Cheng, C. L., Yang, S. X., Yuan, B., Pei, C. L., Zhou, Z. H., Mao, L. Y., Liu, S. L., Chen, D. Y., Cheng, X. Y., Li, M., Shao, M., and Zhou, Z.: The significant contribution of nitrate to a severe haze event in the winter of Guangzhou, China, Sci. Total Environ., 909, https://doi.org/10.1016/j.scitotenv.2023.168582, 2024.

Ehhalt, D. H. and Rohrer, F.: Dependence of the OH concentration on solar UV, J. Geophys. Res.-Atmos., 105, 3565–3571, https://doi.org/10.1029/1999jd901070, 2000.

Fu, X. X., Wang, X. M., Liu, T. Y., He, Q. F., Zhang, Z., Zhang, Y. L., Song, W., Dai, Q. W., Chen, S., and Dong, F. Q.: Secondary inorganic aerosols and aerosol acidity at different $PM_{2.5}$ pollution levels during winter haze episodes in the Sichuan Basin, China, Sci. Total Environ., 918, https://doi.org/10.1016/j.scitotenv.2024.170512, 2024.

Gui, K., Che, H. Z., Zeng, Z. L., Wang, Y. Q., Zhai, S. X., Wang, Z. M., Luo, M., Zhang, L., Liao, T. T., Zhao, H. J., Li, L., Zheng, Y., and Zhang, X. Y.: Construction of a virtual $PM_{2.5}$ observation network in China based on high-density surface meteorological observations using the Extreme Gradient Boosting model, Environ. Int., 141, https://doi.org/10.1016/j.envint.2020.105801, 2020.

Hersbach, H., Bell, B., Berrisford, P., Hirahara, S., Horányi, A., Muñoz-Sabater, J., Nicolas, J., Peubey, C., Radu, R., Schepers, D., Simmons, A., Soci, C., Abdalla, S., Abellan, X., Balsamo, G., Bechtold, P., Biavati, G., Bidlot, J., Bonavita, M., De Chiara, G., Dahlgren, P., Dee, D., Diamantakis, M., Dragani, R., Flemming, J., Forbes, R., Fuentes, M., Geer, A., Haimberger, L., Healy, S., Hogan, R. J., Hólm, E., Janisková, M., Keeley, S., Laloyaux, P., Lopez, P., Lupu, C., Radnoti, G., de Rosnay, P.,

Rozum, I., Vamborg, F., Villaume, S., and Thépaut, J. N.: The ERA5 global reanalysis, Q. J. Roy. Meteor. Soc., 146, 1999–2049, https://doi.org/10.1002/qj.3803, 2020.

Hu, H., Wang, H., Lu, K., Wang, J., Zheng, Z., Xu, X., Zhai, T., Chen, X., Lu, X., Fu, W., Li, X., Zeng, L., Hu, M., Zhang, Y., and Fan, S.: Variation and trend of nitrate radical reactivity towards volatile organic compounds in Beijing, China, Atmos. Chem. Phys., 23, 8211–8223, https://doi.org/10.5194/acp-23-8211-2023, 2023.

Huang, X., Ding, A. J., Wang, Z. L., Ding, K., Gao, J., Chai, F. H., and Fu, C. B.: Amplified transboundary transport of haze by aerosol-boundary layer interaction in China, Nat. Geosci., 13, 428–434, https://doi.org/10.1038/s41561-020-0583-4, 2020.

Jenkin, M. E., Young, J. C., and Rickard, A. R.: The MCM v3.3.1 degradation scheme for isoprene, Atmos. Chem. Phys., 15, 11433–11459, https://doi.org/10.5194/acp-15-11433-2015, 2015.

Lelieveld, J., Evans, J. S., Fnais, M., Giannadaki, D., and Pozzer, A.: The contribution of outdoor air pollution sources to premature mortality on a global scale, Nature. 525, 367–371, https://doi.org/10.1038/nature15371, 2015.

Li, F. B., Huang, D. D., Nie, W., Tham, Y. J., Lou, S. R., Li, Y. Y., Tian, L. H., Liu, Y. L., Zhou, M., Wang, H. C., Qiao, L. P., Wang, H. L., Wang, Z., Huang, C., and Li, Y. J.: Observation of nitrogen oxide-influenced chlorine chemistry and source analysis of Cl_2 in the Yangtze River Delta, China, Atmos. Environ., 306, https://doi.org/10.1016/j.atmosenv.2023.119829, 2023.

Li, M., Zhang, Z., Yao, Q., Wang, T., Xie, M., Li, S., Zhuang, B., and Han, Y.: Nonlinear responses of particulate nitrate to NO_x emission controls in the megalopolises of China, Atmos. Chem. Phys., 21, 15135–15152, https://doi.org/10.5194/acp-21-15135-2021, 2021.

Lin, Z., Xu, L., Yang, C., Chen, G., Ji, X., Li, L., Zhang, K., Hong, Y., Li, M., Fan, X., Hu, B., Zhang, F., and Chen, J.: Trends of peroxyacetyl nitrate and its impact on ozone over 2018–2022 in urban atmosphere, npj Clim. Atmos. Sci., 7, 192, https://doi.org/10.1038/s41612-024-00746-7, 2024.

Lin, Z., Ying, C., Xu, L., Ji, X., Zhang, K., Zhang, F., Chen, G., Li, L., Yang, C., Chen, Y., Chen, Z., Chen, J. Data availability about the measurement report titled "Measurement report: High contribution of N_2O_5 uptake to particulate nitrate formation in NO_2-limited urban areas", figshare [data set], https://doi.org/10.6084/m9.figshare.29670629.v2, 2025.

Liu, M. X., Huang, X., Song, Y., Tang, J., Cao, J. J., Zhang, X. Y., Zhang, Q., Wang, S. X., Xu, T. T., Kang, L., Cai, X. H., Zhang, H. S., Yang, F. M., Wang, H. B., Yu, J. Z., Lau, A. K. H., He, L. Y., Huang, X. F., Duan, L., Ding, A. J., Xue, L. K., Gao, J., Liu, B., and Zhu, T.: Ammonia emission control in China would mitigate haze pollution and nitrogen deposition, but worsen acid rain, P. Natl. Acad. Sci. USA, 116, 7760–7765, https://doi.org/10.1073/pnas.1814880116, 2019.

Liu, T., Hong, Y., Li, M., Xu, L., Chen, J., Bian, Y., Yang, C., Dan, Y., Zhang, Y., Xue, L., Zhao, M., Huang, Z., and Wang, H.: Atmospheric oxidation capacity and ozone pollution mechanism in a coastal city of southeastern China: analysis of a typical photochemical episode by an observation-based model, Atmos. Chem. Phys., 22, 2173–2190, https://doi.org/10.5194/acp-22-2173-2022, 2022.

Liu, Y., Wang, Y., Ma, P., Ma, Y., Pan, Y., Ma, W., Li, S., Liu, P., Liao, Z., Liu, Z., Chu, B., Ma, Q., Quan, J., and He, H.: Formation of Nitrate in the Residual Layer of Beijing: Pathways Evaluation and Contributions to the Ground Level, Environ. Sci. Technol., 59, 9699–9708, https://doi.org/10.1021/acs.est.5c02981, 2025.

Ma, P. K., Quan, J. N., Dou, Y. J., Pan, Y. B., Liao, Z. H., Cheng, Z. G., Jia, X. C., Wang, Q. Q., Zhan, J. L., Ma, W., Zheng, F. X., Wang, Y. Z., Zhang, Y. S., Hua, C. J., Yan, C., Kulmala, M., Liu, Y. A., Huang, X., Yuan, B., Brown, S. S., and Liu, Y. C.: Regime-Dependence of Nocturnal Nitrate Formation via N_2O_5 Hydrolysis and Its Implication for Mitigating Nitrate Pollution, Geophys. Res. Lett., 50, https://doi.org/10.1029/2023gl106183, 2023.

Mao, J. Y., Yan, F. H., Zheng, L. M., You, Y. C., Wang, W. W., Jia, S. G., Liao, W. H., Wang, X. M., and Chen, W. H.: Ozone control strategies for local formation- and regional transport-dominant scenarios in a manufacturing city in southern China, Sci. Total Environ., 813, https://doi.org/10.1016/j.scitotenv.2021.151883, 2022.

McDuffie, E. E., Fibiger, D. L., Dubé, W. P., Hilfiker, F. L., Lee, B. H., Jaeglé, L., Guo, H. Y., Weber, R. J., Reeves, J. M., Weinheimer, A. J., Schroder, J. C., Campuzano-Jost, P., Jimenez, J. L., Dibb, J. E., Veres, P., Ebben, C., Sparks, T. L., Wooldridge, P. J., Cohen, R. C., Campos, T., Hall, S. R., Ullmann, K., Roberts, J. M., Thornton, J. A., and Brown, S. S.: $ClNO_2$ Yields From Aircraft Measurements During the 2015 WINTER Campaign and Critical Evaluation of the Current Parameterization, J. Geophys. Res.-Atmos., 123, 12994–13015, https://doi.org/10.1029/2018jd029358, 2018a.

McDuffie, E. E., Fibiger, D. L., Dubé, W. P., Lopez-Hilfiker, F., Lee, B. H., Thornton, J. A., Shah, V., Jaeglé, L., Guo, H. Y., Weber, R. J., Reeves, J. M., Weinheimer, A. J., Schroder, J. C., Campuzano-Jost, P., Jimenez, J. L., Dibb, J. E., Veres, P., Ebben, C., Sparks, T. L., Wooldridge, P. J., Cohen, R. C., Hornbrook, R. S., Apel, E. C., Campos, T., Hall, S. R., Ullmann, K., and Brown, S. S.: Heterogeneous N_2O_5 Uptake During Winter: Aircraft Measurements During the 2015 WINTER Campaign and Critical Evaluation of Current Parameterizations, J. Geophys. Res.-Atmos., 123, 4345–4372, https://doi.org/10.1002/2018jd028336, 2018b.

McDuffie, E. E., Womack, C. C., Fibiger, D. L., Dube, W. P., Franchin, A., Middlebrook, A. M., Goldberger, L., Lee, B. H., Thornton, J. A., Moravek, A., Murphy, J. G., Baasandorj, M., and Brown, S. S.: On the contribution of nocturnal heterogeneous reactive nitrogen chemistry to particulate matter formation during wintertime pollution events in Northern Utah, Atmos. Chem. Phys., 19, 9287–9308, https://doi.org/10.5194/acp-19-9287-2019, 2019.

Morgan, W. T., Ouyang, B., Allan, J. D., Aruffo, E., Di Carlo, P., Kennedy, O. J., Lowe, D., Flynn, M. J., Rosenberg, P. D., Williams, P. I., Jones, R., McFiggans, G. B., and Coe, H.: Influence of aerosol chemical composition on N_2O_5 uptake: airborne regional measurements in northwestern Europe, Atmos. Chem. Phys., 15, 973–990, https://doi.org/10.5194/acp-15-973-2015, 2015.

Niu, Y. B., Zhu, B., He, L. Y., Wang, Z., Lin, X. Y., Tang, M. X., and Huang, X. F.: Fast Nocturnal Heterogeneous Chemistry in a Coastal Background Atmosphere and Its Implications

for Daytime Photochemistry, J. Geophys. Res.-Atmos., 127, https://doi.org/10.1029/2022jd036716, 2022.

Requia, W. J., Di, Q., Silvern, R., Kelly, J. T., Koutrakis, P., Mickley, L. J., Sulprizio, M. P., Amini, H., Shi, L. H., and Schwartz, J.: An Ensemble Learning Approach for Estimating High Spatiotemporal Resolution of Ground-Level Ozone in the Contiguous United States, Environ. Sci. Technol., 54, 11037–11047, https://doi.org/10.1021/acs.est.0c01791, 2020.

Seinfeld, J. H.: Urban air-pollution – state of the science, Science, 243, 745–752, https://doi.org/10.1126/science.243.4892.745, 1989.

Sun, J., Qin, M., Xie, X., Fu, W., Qin, Y., Sheng, L., Li, L., Li, J., Sulaymon, I. D., Jiang, L., Huang, L., Yu, X., and Hu, J.: Seasonal modeling analysis of nitrate formation pathways in Yangtze River Delta region, China, Atmos. Chem. Phys., 22, 12629–12646, https://doi.org/10.5194/acp-22-12629-2022, 2022.

Thaler, R. D., Mielke, L. H., and Osthoff, H. D.: Quantification of Nitryl Chloride at Part Per Trillion Mixing Ratios by Thermal Dissociation Cavity Ring-Down Spectroscopy, Anal. Chem., 83, 2761–2766, https://doi.org/10.1021/ac200055z, 2011.

Tham, Y. J., Wang, Z., Li, Q., Yun, H., Wang, W., Wang, X., Xue, L., Lu, K., Ma, N., Bohn, B., Li, X., Kecorius, S., Größ, J., Shao, M., Wiedensohler, A., Zhang, Y., and Wang, T.: Significant concentrations of nitryl chloride sustained in the morning: investigations of the causes and impacts on ozone production in a polluted region of northern China, Atmos. Chem. Phys., 16, 14959–14977, https://doi.org/10.5194/acp-16-14959-2016, 2016.

Tham, Y. J., Wang, Z., Li, Q., Wang, W., Wang, X., Lu, K., Ma, N., Yan, C., Kecorius, S., Wiedensohler, A., Zhang, Y., and Wang, T.: Heterogeneous N_2O_5 uptake coefficient and production yield of $ClNO_2$ in polluted northern China: roles of aerosol water content and chemical composition, Atmos. Chem. Phys., 18, 13155–13171, https://doi.org/10.5194/acp-18-13155-2018, 2018.

Wagner, N. L., Riedel, T. P., Young, C. J., Bahreini, R., Brock, C. A., Dubé, W. P., Kim, S., Middlebrook, A. M., Öztürk, F., Roberts, J. M., Russo, R., Sive, B., Swarthout, R., Thornton, J. A., VandenBoer, T. C., Zhou, Y., and Brown, S. S.: N_2O_5 uptake coefficients and nocturnal NO_2 removal rates determined from ambient wintertime measurements, J. Geophys. Res.-Atmos., 118, 9331–9350, https://doi.org/10.1002/jgrd.50653, 2013.

Wang, H., Lu, K., Guo, S., Wu, Z., Shang, D., Tan, Z., Wang, Y., Le Breton, M., Lou, S., Tang, M., Wu, Y., Zhu, W., Zheng, J., Zeng, L., Hallquist, M., Hu, M., and Zhang, Y.: Efficient N_2O_5 uptake and NO_3 oxidation in the outflow of urban Beijing, Atmos. Chem. Phys., 18, 9705–9721, https://doi.org/10.5194/acp-18-9705-2018, 2018.

Wang, H., Peng, C., Wang, X., Lou, S., Lu, K., Gan, G., Jia, X., Chen, X., Chen, J., Wang, H., Fan, S., Wang, X., and Tang, M.: N_2O_5 uptake onto saline mineral dust: a potential missing source of tropospheric $ClNO_2$ in inland China, Atmos. Chem. Phys., 22, 1845–1859, https://doi.org/10.5194/acp-22-1845-2022, 2022a.

Wang, H., Yuan, B., Zheng, E., Zhang, X., Wang, J., Lu, K., Ye, C., Yang, L., Huang, S., Hu, W., Yang, S., Peng, Y., Qi, J., Wang, S., He, X., Chen, Y., Li, T., Wang, W., Huangfu, Y., Li, X., Cai, M., Wang, X., and Shao, M.: Formation and impacts of nitryl chloride in Pearl River Delta, Atmos. Chem. Phys., 22, 14837–14858, https://doi.org/10.5194/acp-22-14837-2022, 2022b.

Wang, H. C., Lu, K. D., Chen, X. R., Zhu, Q. D., Chen, Q., Guo, S., Jiang, M. Q., Li, X., Shang, D. J., Tan, Z. F., Wu, Y. S., Wu, Z. J., Zou, Q., Zheng, Y., Zeng, L. M., Zhu, T., Hu, M., and Zhang, Y. H.: High N_2O_5 Concentrations Observed in Urban Beijing: Implications of a Large Nitrate Formation Pathway, Environ. Sci. Technol. Letters. 4, 416–420, https://doi.org/10.1021/acs.estlett.7b00341, 2017.

Wang, H. C., Lu, K. D., Chen, S. Y., Li, X., Zeng, L. M., Hu, M., and Zhang, Y. H.: Characterizing nitrate radical budget trends in Beijing during 2013–2019, Sci. Total Environ., 795, https://doi.org/10.1016/j.scitotenv.2021.148869, 2021.

Wang, W. J., Li, X., Cheng, Y. F., Parrish, D. D., Ni, R. J., Tan, Z. F., Liu, Y., Lu, S. H., Wu, Y. S., Chen, S. Y., Lu, K. D., Hu, M., Zeng, L. M., Shao, M., Huang, C., Tian, X. D., Leung, K. M., Chen, L. F., Fan, M., Zhang, Q., Rohrer, F., Wahner, A., Pöschl, U., Su, H., and Zhang, Y. H.: Ozone pollution mitigation strategy informed by long-term trends of atmospheric oxidation capacity, Nat. Geosci., 16, 1080–1081, https://doi.org/10.1038/s41561-023-01334-9, 2023a.

Wang, Y. H., Gao, W. K., Wang, S., Song, T., Gong, Z. Y., Ji, D. S., Wang, L. L., Liu, Z. R., Tang, G. Q., Huo, Y. F., Tian, S. L., Li, J. Y., Li, M. G., Yang, Y., Chu, B. W., Petäjä, T., Kerminen, V. M., He, H., Hao, J. M., Kulmala, M., Wang, Y. S., and Zhang, Y. H.: Contrasting trends of $PM_{2.5}$ and surface-ozone concentrations in China from 2013 to 2017, Natl. Sci. Rev., 7, 1331–1339, https://doi.org/10.1093/nsr/nwaa032, 2020.

Wang, Y. R., Yang, X. Y., Wu, K., Mei, H., De Smedt, I., Wang, S. G., Fan, J., Lyu, S., and He, C.: Long-term trends of ozone and precursors from 2013 to 2020 in a megacity (Chengdu), China: Evidence of changing emissions and chemistry, Atmos. Res., 278, https://doi.org/10.1016/j.atmosres.2022.106309, 2022c.

Wang, Y. T., Zhao, Y., Liu, Y. M., Jiang, Y. Q., Zheng, B., Xing, J., Liu, Y., Wang, S., and Nielsen, C. P.: Sustained emission reductions have restrained the ozone pollution over China, Nat. Geosci., 16, 967–974, https://doi.org/10.1038/s41561-023-01284-2, 2023b.

Wen, L., Xue, L., Wang, X., Xu, C., Chen, T., Yang, L., Wang, T., Zhang, Q., and Wang, W.: Summertime fine particulate nitrate pollution in the North China Plain: increasing trends, formation mechanisms and implications for control policy, Atmos. Chem. Phys., 18, 11261–11275, https://doi.org/10.5194/acp-18-11261-2018, 2018.

Wolfe, G. M., Marvin, M. R., Roberts, S. J., Travis, K. R., and Liao, J.: The Framework for 0-D Atmospheric Modeling (F0AM) v3.1, Geosci. Model Dev., 9, 3309–3319, https://doi.org/10.5194/gmd-9-3309-2016, 2016.

Xie, X. D., Hu, J. L., Qin, M. M., Guo, S., Hu, M., Wang, H. L., Lou, S. R., Li, J. Y., Sun, J. J., Li, X., Sheng, L., Zhu, J. L., Chen, G. Y., Yin, J. J., Fu, W. X., Huang, C., and Zhang, Y. H.: Modeling particulate nitrate in China: Current findings and future directions, Environ. Int., 166, https://doi.org/10.1016/j.envint.2022.107369, 2022.

Xing, J., Ding, D., Wang, S., Zhao, B., Jang, C., Wu, W., Zhang, F., Zhu, Y., and Hao, J.: Quantification of the enhanced effectiveness of NO_x control from simultaneous reductions of VOC and NH_3 for reducing air pollution in the Beijing–Tianjin–Hebei region, China, Atmos. Chem. Phys., 18, 7799–7814, https://doi.org/10.5194/acp-18-7799-2018, 2018.

Yan, C., Tham, Y. J., Nie, W., Xia, M., Wang, H. C., Guo, Y. S., Ma, W., Zhan, J. L., Hua, C. J., Li, Y. Y., Deng, C. J., Li, Y. R., Zheng, F. X., Chen, X., Li, Q. Y., Zhang, G., Mahajan, A. S., Cuevas, C. A., Huang, D. D., Wang, Z., Sun, Y. L., Saiz-Lopez, A., Bianchi, F., Kerminen, V. M., Worsnop, D. R., Donahue, N. M., Jiang, J. K., Liu, Y. C., Ding, A. J., and Kulmala, M.: Increasing contribution of nighttime nitrogen chemistry to wintertime haze formation in Beijing observed during COVID-19 lockdowns, Nat. Geosci., 16, 975–981, https://doi.org/10.1038/s41561-023-01285-1, 2023.

Yang, C., Dong, H. S., Chen, Y. P., Xu, L. L., Chen, G. J., Fan, X. L., Wang, Y. H., Tham, Y. J., Lin, Z. Y., Li, M. R., Hong, Y. W., and Chen, J. S.: New Insights on the Formation of Nucleation Mode Particles in a Coastal City Based on a Machine Learning Approach, Environ. Sci. Technol., 58, 1187–1198, https://doi.org/10.1021/acs.est.3c07042, 2023.

Yang, S., Yuan, B., Peng, Y., Huang, S., Chen, W., Hu, W., Pei, C., Zhou, J., Parrish, D. D., Wang, W., He, X., Cheng, C., Li, X.-B., Yang, X., Song, Y., Wang, H., Qi, J., Wang, B., Wang, C., Wang, C., Wang, Z., Li, T., Zheng, E., Wang, S., Wu, C., Cai, M., Ye, C., Song, W., Cheng, P., Chen, D., Wang, X., Zhang, Z., Wang, X., Zheng, J., and Shao, M.: The formation and mitigation of nitrate pollution: comparison between urban and suburban environments, Atmos. Chem. Phys., 22, 4539–4556, https://doi.org/10.5194/acp-22-4539-2022, 2022.

Yu, C., Wang, Z., Xia, M., Fu, X., Wang, W., Tham, Y. J., Chen, T., Zheng, P., Li, H., Shan, Y., Wang, X., Xue, L., Zhou, Y., Yue, D., Ou, Y., Gao, J., Lu, K., Brown, S. S., Zhang, Y., and Wang, T.: Heterogeneous N_2O_5 reactions on atmospheric aerosols at four Chinese sites: improving model representation of uptake parameters, Atmos. Chem. Phys., 20, 4367–4378, https://doi.org/10.5194/acp-20-4367-2020, 2020.

Yun, H., Wang, W., Wang, T., Xia, M., Yu, C., Wang, Z., Poon, S. C. N., Yue, D., and Zhou, Y.: Nitrate formation from heterogeneous uptake of dinitrogen pentoxide during a severe winter haze in southern China, Atmos. Chem. Phys., 18, 17515–17527, https://doi.org/10.5194/acp-18-17515-2018, 2018.

Zhai, S. X., Jacob, D. J., Wang, X., Liu, Z. R., Wen, T. X., Shah, V., Li, K., Moch, J. M., Bates, K. H., Song, S. J., Shen, L., Zhang, Y. Z., Luo, G., Yu, F. Q., Sun, Y. L., Wang, L. T., Qi, M. Y., Tao, J., Gui, K., Xu, H. H., Zhang, Q., Zhao, T. L., Wang, Y. S., Lee, H. C., Choi, H., and Liao, H.: Control of particulate nitrate air pollution in China, Nat. Geosci., 14, 389–395, https://doi.org/10.1038/s41561-021-00726-z, 2021.

Zhai, T., Lu, K., Wang, H., Lou, S., Chen, X., Hu, R., and Zhang, Y.: Elucidate the formation mechanism of particulate nitrate based on direct radical observations in the Yangtze River Delta summer 2019, Atmos. Chem. Phys., 23, 2379–2391, https://doi.org/10.5194/acp-23-2379-2023, 2023.

Zhang, R., Han, Y. H., Shi, A. J., Sun, X. S., Yan, X., Huang, Y. H., and Wang, Y.: Characteristics of ambient ammonia and its effects on particulate ammonium in winter of urban Beijing, China, Environ. Sci. Pollut. R., 28, 62828–62838, https://doi.org/10.1007/s11356-021-14108-w, 2021.

Zhang, X., Ma, Q., Chu, W. H., Ning, M., Liu, X. Q., Xiao, F. J., Cai, N. N., Wu, Z. J., and Yan, G.: Identify the key emission sources for mitigating ozone pollution: A case study of urban area in the Yangtze River Delta region, China, Sci. Total Environ., 892, https://doi.org/10.1016/j.scitotenv.2023.164703, 2023a.

Zhang, Y., Lei, R., Cui, S., Wang, H., Chen, M., and Ge, X.: Spatiotemporal trends and impact factors of $PM_{2.5}$ and O_3 pollution in major cities in China during 2015–2020, Chinese Sci. Bull., 67, 2029–2042, 2022.

Zhang, Y. N., Wang, H. L., Huang, L. B., Qiao, L. P., Zhou, M., Mu, J. S., Wu, C., Zhu, Y. J., Shen, H. Q., Huang, C., Wang, G. H., Wang, T., Wang, W. X., and Xue, L. K.: Double-Edged Role of VOCs Reduction in Nitrate Formation: Insights from Observations during the China International Import Expo 2018, Environ. Sci. Technol., 57, 15979–15989, https://doi.org/10.1021/acs.est.3c04629, 2023b.

Zhao, S. P., Yin, D. Y., Yu, Y., Kang, S. C., Qin, D. H., and Dong, L. X.: $PM_{2.5}$ and O_3 pollution during 2015–2019 over 367 Chinese cities: Spatiotemporal variations, meteorological and topographical impacts, Environ. Pollut., 264, https://doi.org/10.1016/j.envpol.2020.114694, 2020.

Zhao, X. X., Zhao, X. J., Liu, P. F., Chen, D., Zhang, C. L., Xue, C. Y., Liu, J. F., Xu, J., and Mu, Y. J.: Transport Pathways of Nitrate Formed from Nocturnal N_2O_5 Hydrolysis Aloft to the Ground Level in Winter North China Plain, Environ. Sci. Technol., https://doi.org/10.1021/acs.est.3c00086, 2023.

Zhou, M., Nie, W., Qiao, L. P., Huang, D. D., Zhu, S. H., Lou, S. R., Wang, H. L., Wang, Q., Tao, S. K., Sun, P., Liu, Y. W., Xu, Z., An, J. Y., Yan, R. S., Su, H., Huang, C., Ding, A. J., and Chen, C. H.: Elevated Formation of Particulate Nitrate From N_2O_5 Hydrolysis in the Yangtze River Delta Region From 2011 to 2019, Geophys. Res. Lett., 49, https://doi.org/10.1029/2021gl097393, 2022.

Zong, Z., Tian, C. G., Sun, Z. Y., Tan, Y., Shi, Y. J., Liu, X. H., Li, J., Fang, Y. T., Chen, Y. J., Ma, Y. H., Gao, H. W., Zhang, G., and Wang, T.: Long-Term Evolution of Particulate Nitrate Pollution in North China: Isotopic Evidence From 10 Offshore Cruises in the Bohai Sea From 2014 to 2019, J. Geophys. Res.-Atmos., 127, https://doi.org/10.1029/2022jd036567, 2022.